THE JOURNAL OF PHYSICAL CHEMISTRY B

Article

pubs.acs.org/JPCB

Two-Photon Absorption-Molecular Structure Investigation Using a Porphycene Chromophore with Potential in Photodynamic Therapy

L. Therese Bergendahl and Martin J. Paterson*

Institute of Chemical Sciences, Heriot Watt University, Edinburgh, EH14 4AS, United Kingdom

ABSTRACT: Porphycenes have been shown to exhibit many advantageous properties when it comes to the application of two-photon absorption (TPA), a technique with potential use in the area of photodynamic therapy (PDT). A computational study of structure−reactivity relationships in the one- and two-photon absorption spectra of a series of 2,7,12,17-substituted porphycenes has been carried out using linear and quadratic density functional response theory. The focus has been on determining the effect on the spectra of electron donating and withdrawing substituents, the outcome of extending the conjugation lengths to these substituents, and the consequence of formation of metallo-porphycene complexes. In particular, we have looked at the use of TPA in order to improve the penetration depth of the therapeutic light dose, in terms of the position of the absorption maximum with respect to the optical window of tissue penetration, as well as the effect on the TPA cross section. The extent of conjugation was shown to be particularly crucial for increasing the TPA cross section, for both the electron withdrawing and donating substituents, while the inclusion of a metal in the center of the macrocycle was shown to benefit the absorption wavelength in terms of tissue penetration considerations.

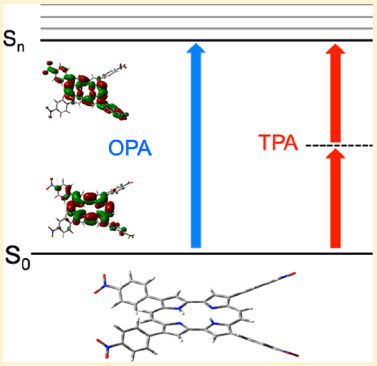

INTRODUCTION

The phenomenon of two-photon absorption (TPA) has, over the last couple of decades, evolved from being a curious optical effect to a technique with enormous potential in a number of areas including 3D optical storage, in vivo fluorescense imaging, and photodynamic therapy (PDT).[1−6] In PDT, TPA is utilized to excite a photosensitizer chromophore which subsequently, through an energy transfer process, will generate the reactive singlet oxygen species, $O_2(a^1\Delta_g)$. Singlet oxygen is a compound crucial for the activation of the programmed cell death pathway in biological systems, and this destructive nature is desired in the use of PDT as an anticancer treatment.[7−10] The photosensitization pathway taking place within a target cell is illustrated in the modified Jablonski diagram in Figure 1. After excitation of the photosensitizer, either through one-photon absorption (OPA) or TPA, radiation-less spin−orbit coupling dependent ISC can occur to a close-lying triplet state which subsequently has a high probability of being quenched by ground state oxygen.

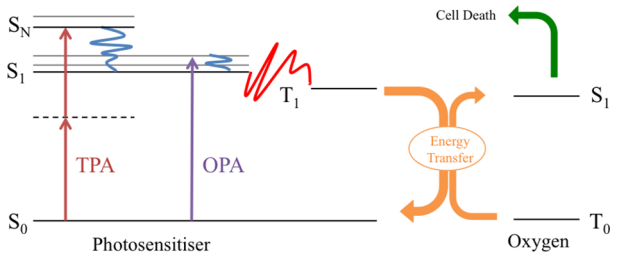

Figure 1. Modified Jablonski diagram indicating the energy flow from the excited photosensitizer species, achieved through either one- or two-photon absorption, leading to the generation of singlet oxygen, and subsequent cell death. The dashed horizontal line represents a virtual state.

The use of a non-linear optical excitation technique such as TPA does not necessarily have an impact on the subsequent ISC or singlet oxygen generation by the molecule but can still provide numerous advantages in this field.[11−14] It is, for example, evident that a molecule with a center of inversion will have states available for TPA that diverge from those available for conventional OPA, resulting from a change in parity selection rules for the transition, potentially accessing states that are dark with respect to OPA. However, it is worth noting that systems with a center of inversion might not necessarily have overlapping OPA and TPA transitions.[15] A further advantage with a non-linear excitation process is the fact that the probability of TPA falls off quadratically with respect to the focus of the excitation source, e.g., a focused laser beam. The singlet oxygen production can therefore be restricted to a very small volume, and thus, extremely high spatial resolution for PDT treatment can be achieved. However, the main advantage of this technique is arguably the fact that the non-linear absorption process takes place using two photons to achieve an excitation that normally requires one higher energy/shorter wavelength photon. This highlights an avenue by which the photosensitizer can be designed toward absorption in the optimum position in the optical window of tissue penetration, at 650−1300 nm. In this wavelength region, the absorption due to chromophores such as hemoglobin, melanin, and water is at

Received: May 24, 2012
Revised: August 31, 2012
Published: September 4, 2012

dx.doi.org/10.1021/jp305063e | J. Phys. Chem. B 2012, 116, 11818−11828

a minimum. Even though developments in PDT have not yet resulted in its general use as an anticancer therapy, it is still an exceptionally attractive goal and research continues today along many promising avenues. It is a relative non-invasive therapy that also benefits from many opportunities of targeted treatment, both through the targeting of the photosensitizer chromophore as well as the light dosage. One of the main limitations with current photosensitizers, and the use of PDT as a routine anticancer therapy, is the difficulty involved in the delivery of the radiation dose. Chromophores absorbing in the tissue transparency wavelength region would therefore be of great value in future photosensitizer development.

Among the molecules under investigation for their general applicability as photosensitizing agents in PDT, the family of *porphyrin* related structures is the most studied, and the first PDT photosensitizer agent to reach the market was indeed a porphyrin derivative, *Photofrin*.[16] The non-linear optical properties of porphyrin derivatives have also been investigated comparatively extensively. The reduced porphyrin isomer *porphycene*, however, has been less studied despite its promising TPA characteristics. Porphycene (**Pc**) was the first porphyrin isomer to be synthesized, in the late 1960s, and theoretical, as well as experimental, results show that the **Pc** system has a very strong TPA compared to porphyrin analogues in the same spectral region, due to one-photon resonance enhanced absorption (*vide infra*), and as such, it is a promising molecular starting point for a study into the effects of systematic structural variations on its TPA spectra.[15,17−20]

The tools and methods for the theoretical modeling of materials, and their linear and non-linear optical properties, have been under rapid development in the last couple of decades. Recent improvements in methods capable of modeling large many-electron systems, such as *density functional theory* (DFT), and in particular DFT functionals for use in *response theory*, mean it is now possible to calculate accurate TPA spectra for relatively large molecules from first principles, without the need for expensive large sum-over-states methods.[21−24] As many two-photon absorbing chromophores that could be promising as photosensitizers for potential future use in PDT are time-consuming as well as costly to develop, theoretical predictions of structure−TPA relationships are of great importance.

The probability of TPA in any molecular system is defined through its TPA cross section, δ, which is controlled by the molecular electronic structure. When improving the two-photon absorbing quality of a molecular system, general strategies that have previously demonstrated to be useful have been to maximize the magnitudes of the dipole moment of the transition as well as the difference in permanent dipole moments of the ground and excited states. A molecular structure that promotes intramolecular charge transfer is therefore crucial. The presence of an electron donor as well as an acceptor region in the chromophore is thus very beneficial, as is the increase in path length of the charge transfer, through extension of a π-system, as it results in states with large permanent dipoles.[25−31] A further strategy to increase the TPA response is coordination of the relevant chromophore to a metal center, which has been shown to increase permanent dipole charge differences, as well as enhance the probability of spin−orbit coupling dependent ISC.[32−34]

In this study, we have chosen to investigate the TPA qualities of the **Pc** macrocycle with electron acceptor or donor groups attached with and without an extended π-bridge. The derivatives were designed with 2,7,12,17-nitrophenyl substituents as strong electron acceptors (**PcPN**) and 2,7,12,17-dimethylamine substituents as strong electron donors (**PcDMA**), as they have been demonstrated previously to increase the TPA cross section in a variety of chromophores. A phenyl-bridge was chosen to extend the π-system and promote charge transfer through the structure. We also investigated the effects of the coordination of the macrocycle to a Zn and Pd metal center. The addition of Zn has shown to be beneficial in OPA PDT using the phthalocyanine photosensitizer, both in improving its OPA absorption as well as the facilitation of greater cellular uptake. Inclusion of Pd was chosen both due to its common usage in numerous experimental assays for the study of O_2 phosphorescence, as well as a starting point for future studies into its effects on internal pathways such as ISC in the photosensitizer. The **Pc** derivatives were designed as per Scheme 1, in order to illustrate how the systematic change in molecular structure ultimately affects the TPA cross section.

Scheme 1. The Systematic Design of the Photosensitizers Investigated in This Study, Specifying External Substituents, Degree of Extended Conjugation in Terms of the Number of Phenyl Moieties Used, and the Coordination of the Central Core

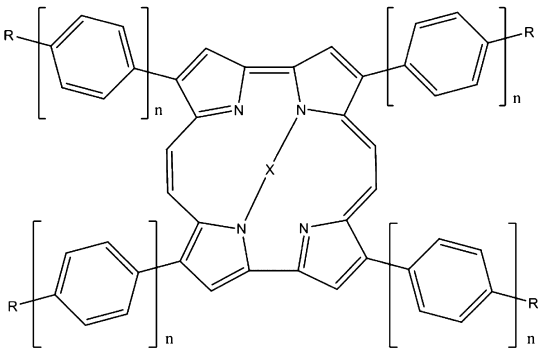

Compound	R	n	X
PcPN	PN	0	2H
PcCPN	PN	1	2H
ZnPcPN	PN	0	Zn
ZnPcCPN	PN	1	Zn
PdPcPN	PN	0	Pd
PdPcCPN	PN	1	Pd
PcDMN	DMN	0	2H
PcCDMN	DMN	1	2H
ZnPcDMN	DMN	0	Zn
ZnPcCDMN	DMN	1	Zn
PdPcDMN	DMN	0	Pd
PdPcCDMN	DMN	1	Pd

DFT was used to optimize the molecular structures on the ground state potential energy surface to identify any global or local minima conformations of the molecular geometries. Thereafter, the vertical excitation OPA and TPA spectra were computed using linear and quadratic DFT response theory, respectively. The applicability of the chosen structures as photosensitizer agents for use in a biological environment was then further investigated by calculations of the OPA spectra with the systems immersed in a polarizable continuum solvent

dx.doi.org/10.1021/jp305063e | J. Phys. Chem. B 2012, 116, 11818−11828

through the use of the PCM method. This method has been shown to be successful in combination with linear response DFT for reproducing optical spectra in solution.[35,36]

COMPUTATIONAL DETAILS

The ground state geometries of each molecular system were optimized using the hybrid B3LYP exchange-correlation functional with the 6-31G* Pople-type basis set on all atoms apart from the metal atoms where the relativistic Stuttgart/Dresden (SDD) pseudopotential was applied for the core electrons and the corresponding basis set for the valence electrons.[37−39] Analytical Hessian calculations were performed to confirm the nature of the stationary point.

At each confirmed ground state optimized geometry, one- and two-photon absorption spectra were computed using linear response and quadratic response DFT, respectively. All geometry optimizations and OPA linear response calculations were computed using Gaussian 09,[40] while TPA quadratic response theory calculations were performed using a local version of the Dalton 2.0 program.[41]

The linear response calculations were carried out with the Coulomb-attenuated version of the Becke three-parameter hybrid B3LYP functional, CAM-B3LYP.[42] This functional allows for a variable degree of exact Hartree−Fock exchange to be added depending on interelectronic distances. This feature gives a better description of the long-range exchange potential than local GGA hybrid functionals do, and it has also been shown to improve the determination of various properties, crucially charge transfer excitation energies, compared to B3LYP, without a significant increase in computational cost.[43,44] The CAM-B3LYP functional was also employed in the quadratic response calculations after a recent study showed that the TPA results calculated using this functional are very reliable when comparing with high level coupled-cluster calculations.[45] This is due to the ability of this functional to describe the intermediate states of the two-photon absorption in a robust and accurate manner, without the method involving the actual calculation of each state explicitly. In response theory calculations, the OPA spectra are obtained from the linear response function and the TPA spectra from the quadratic response function, which both have poles at the excitation energies of the system. The residues of the response functions give the transition moments to the excited states. The residues of the quadratic response function for absorption of two identical photons are equivalent to the two-photon transition tensor, T, which is used to obtain the TPA cross section, δ, as a rotationally averaged quantity.

$$\delta = F\delta^F + G\delta^G + H\delta^H \tag{1}$$

$$\delta^F = \frac{1}{30}\sum_{\alpha,\beta} T_{\alpha,\alpha}T^*_{\beta,\beta}$$

$$\delta^G = \frac{1}{30}\sum_{\alpha,\beta} T_{\alpha,\beta}T^*_{\alpha,\beta}$$

$$\delta^F = \frac{1}{30}\sum_{\alpha,\beta} T_{\alpha,\beta}T^*_{\beta,\alpha}$$

The values F, G, and H depend on the polarization of the incident photons, and the condition applied in this work was linear polarization, where $F = G = H = 2$. In order to discuss the obtained TPA results, it is convenient to express the spatially dependent components of the two-photon transition tensor in a sum-over-states expression for the transition between the ground, 0, intermediate, v, and final states, f, as in eq 2. This expression for the TPA transition tensor is derived from the first residue of the quadratic response function and identical to the general multiphoton transition moment.

$$T_{\alpha,\beta} = \sum_{v=0} \frac{\langle 0|\mu_\alpha|v\rangle\langle v|\mu_\beta|f\rangle}{\omega_v - \omega} + \frac{\langle 0|\mu_\beta|v\rangle\langle v|\mu_\alpha|f\rangle}{\omega_v - \omega} \tag{2}$$

where ω is the frequency of the irradiating light and ω_v is the excitation frequency of the intermediate state v. The labels α and β refer to the Cartesian coordinates x, y, and z of the TPA tensor. The linear combination of all (real) intermediate eigenstates can be thought of as representing a virtual state, as shown in Figure 1, when the ground state is excluded from the summation. Thus robust functionals, such as CAM-B3LYP, are essential, as they need to be able to describe transitions involving a variety of different intermediate states, for example, states with both valence and charge transfer character. Even though the machinery of response theory results in the TPA transition tensor directly, without the need to sum over all states explicitly, this expression is useful for results analysis (*vide infra*).

When considering calculations of molecular properties, the nature of the perturbation needs to be considered when choosing a basis set, and as the absorption of radiation depends on the polarizability of the electron cloud, polarization functions are considered important. However, one would expect the importance of diffuse functions to diminish as one increases the number of basis functions as the chromophore becomes larger. In order to see how well this statement applied in our case and to get a suitable reference for our calculations, we chose the relatively simple 6-31G* as the basis set on the light atoms for a linear response calculation on the **Pc** core and compared with a basis with diffuse functions. As can be seen from Table 1, the 6-31G* basis reproduces state ordering, energy, and oscillator strength results from the diffuse function basis, up to 240 nm, and hence describes well the important Soret- and Q-regions (*vide infra*). 6-31G* was therefore used for all light atoms, as it was expected to provide a suitable balance between computational cost and accuracy.

The results achieved from a linear response calculation, apart from excitation energies, are a set of excitation amplitudes that describe the contribution of a particle−hole pair to the specific transition. In order to analyze the nature of the electronic transitions in detail, natural transition orbitals (NTOs) were calculated for each transition. A NTO is a calculated orbital representation of the electronic transition where transition amplitudes have been reduced to a set of particle−hole amplitudes, in terms of eigenvectors of the transition density matrix, which gives a more intuitive picture of the nature of the transition.[46] The NTO representation of the nature of the excitation is complementary to the response eigenvectors using the Kohn−Sham orbitals but generally gives a more compact representation of the state. In order to assist in the interpretation of the excited states data, a NTO representation was calculated for each excited state of interest from the linear calculations.

In order to simulate solvent interactions, the polarizable continuum model (PCM) was utilized in which the calculation is carried out within a cavity surrounded by a reaction field from the solvent. The solvent was specified as water using the

Table 1. Resulting OPA Spectrum from a Basis Set Comparison on the Pc Core

6-31G*			
wavelength (nm)	energy (eV)	oscillator strength	symmetry
575.5	2.1959	0.156200	^1B_u
541.32	2.3198	0.239200	^1B_u
359.35	3.544	0.000000	^1A_g
354.09	3.5741	0.013600	^1B_u
312.72	3.9986	0.768500	^1B_u
306.82	4.0758	0.730200	^1B_u
299.92	4.1794	0.000000	^1A_g
297.35	4.2082	0.000000	^1B_g
290.48	4.3316	0.000000	^1A_u
286.04	4.3916	0.550600	^1B_u
265.65	4.7237	0.000000	^1A_g
248.69	5.0323	0.000000	^1A_g
238.71	5.2495	0.000000	^1A_g
aug-cc-pVDZ			
wavelength (nm)	energy (eV)	oscillator strength	symmetry
583.34	2.1254	0.148900	^1B_u
553.91	2.2383	0.227100	^1B_u
358.66	3.4569	0.000000	^1A_g
356.84	3.4745	0.034000	^1B_u
320.78	3.8651	0.776000	^1B_u
314.14	3.9468	0.912900	^1B_u
301.19	4.1164	0.000000	^1A_g
296.5	4.1816	0.000000	^1B_g
289.37	4.2846	0.000000	^1A_u
287.67	4.3099	0.363400	^1B_u
268.45	4.6185	0.000000	^1A_g
252.96	4.9014	0.000000	^1A_g
242.61	5.1105	0.000000	^1A_g

standard dielectric constants of Gaussian 09, and non-equilibrium solvation was used in order to avoid the solvent adjusting to the excited state geometry. The solvatochromic effects determined lead to information regarding shifts in the absorption bands, in both OPA and TPA, but the effect on intensity profiles is determined only for OPA. The calculation including solvent effects on TPA is not determined here, although the methods exist.[47−49]

RESULTS AND DISCUSSION

Geometry Optimization. Initially, a rotomer investigation was carried out, in order to inspect the effect of various rotomers of the selected compounds on the absorption spectra. A model system, represented by **PcPN**, was manipulated by varying the starting dihedral angles between the plane of the macrocyclic core and the plane of the substituents, as described in Scheme 2. The ground state energy differences between the various rotomer conformations were found to be very small. Each rotomer was subsequently investigated for OPA and TPA; the differences in the investigated spectra were also found to be very small, and the molecules studied were a combination of all conformers.

Key parameters of the optimization results are presented in Scheme 3. The minimum energy geometry that was found for the free porphycene macrocycle revealed a structure that is completely flat and of C_{2h} symmetry. In the geometries of lowest energy in the optimization calculations for the further

Scheme 2. Overview of the Structure of PcPN with the Angles Manipulated in the Rotomer Investigation Indicated[a]

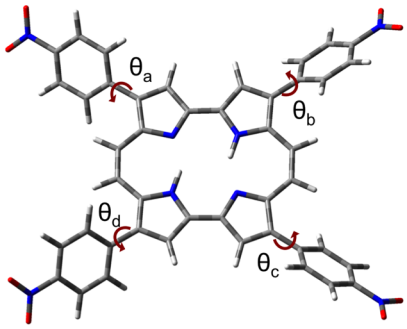

Compound	Starting Angles				Optimised Angles				ΔE
	a	b	c	d	a	b	c	d	
PcPN-1	90	90	90	90	137	42	45	136	0
PcPN-2	135	135	45	135	134	137	44	138	7×10^{-5}
PcPN-3	45	45	135	135	44	45	134	137	2×10^{-4}
PcPN-4	135	45	135	135	135	44	134	137	7×10^{-5}

[a]The relative optimized energies (a.u.) and initial and final angles of the optimized rotomer conformers are tabulated.

Scheme 3. PcCPN and PcCDMN with Angles Indicated to Demonstrate Selected Geometrical Parameters of the Chromophores in This Study

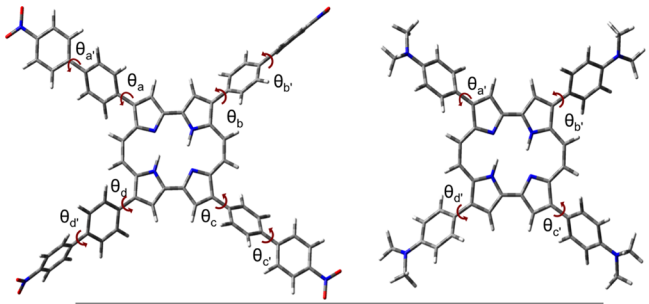

Compound	Angles								Point Group
	a	b	c	d	a'	b'	c'	d'	
Pc									D_{2h}
PcPN	46	43	46	43					C_2
PcCPN	45	44	45	44	37	-36	37	-36	C_2
ZnPcPN	46	45	136	44					C_1
ZnPcCPN	46	44	46	44	36	37	-36	-36	C_3
PdPcPN	47	45	136	44					C_1
PdPcCPN	47	45	47	45	37	37	37	37	D_2
PcDMA									C_1
PcCDMA					42	40	42	40	C_2
ZnPcDMA									C_1
ZnPcCDMA					42	42	42	42	D_2
PdPcDMA									C_1
PdPcCDMA					43	43	43	43	D_2

molecular systems, a twist can be seen in the porphycene center, leaving it non-planar and non-centrosymmetric. The out of plane twist is not very profound in the cases where the macrocycle is coordinated to a metal, although it is still evident. The non-planarity does not effect the symmetries of the systems, and they transform according to the elements of their respective point groups (Figure 2).

One-Photon Absorption. The OPA transitions, from the linear response CAM-B3LYP/6-31G*,SDD computation, were calculated for the first 20 excited states from the optimized geometries on the ground state potential energy surface for each system. The resulting spectra for the free base **Pc** macrocycle and the various derivatives are displayed in Figure 3, and upon analysis, it is evident that nearly all the compounds

dx.doi.org/10.1021/jp305063e | J. Phys. Chem. B 2012, 116, 11818−11828

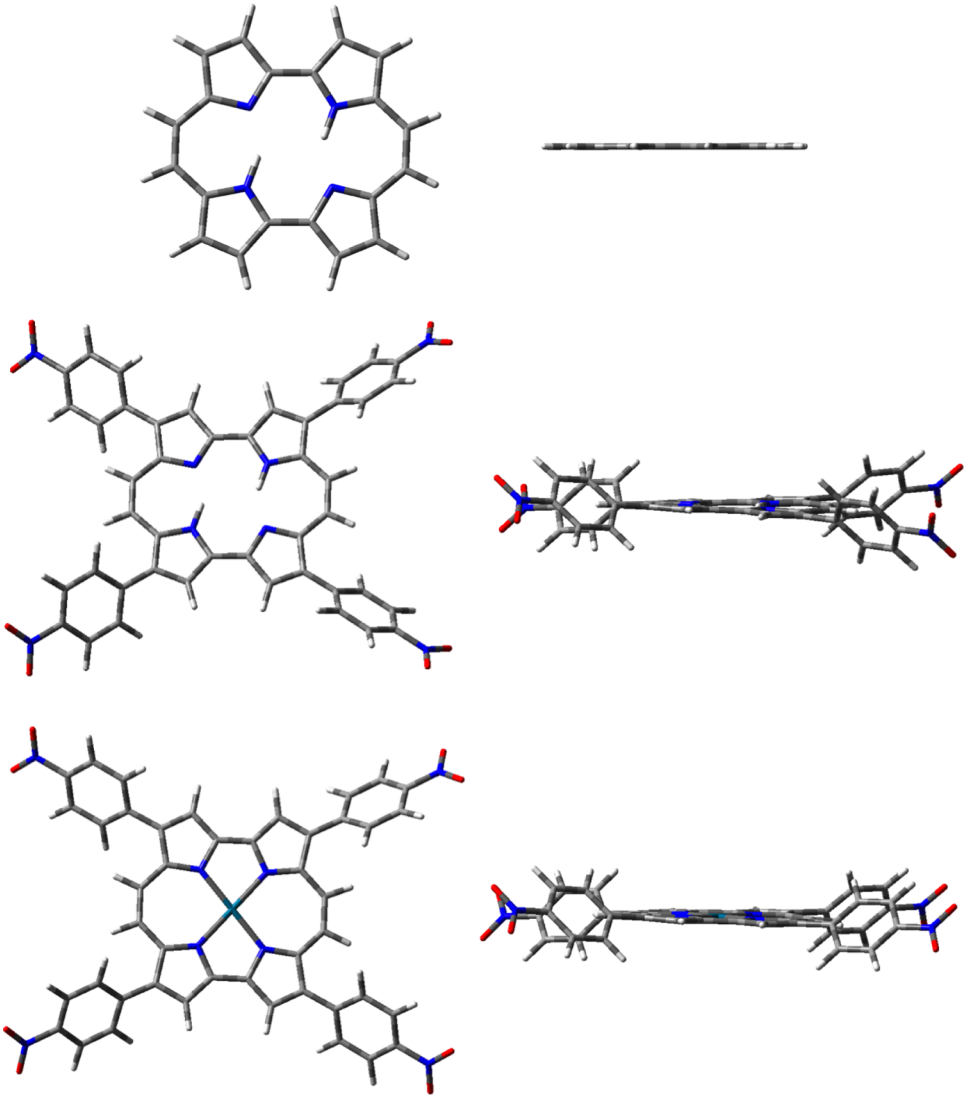

Figure 2. Optimized geometries of **Pc**, **PcPN**, and **PdPcPN**.

have two dominant regions of absorption, one at 300−400 nm and one at 550−650 nm. These two regions of intense absorption are common for many molecules in the porphyrin family, and they are termed the Soret- and *Q*-regions, respectively, according to the classic Gouterman four orbital (GFO) model proposed by Martin Gouterman.[50] According to the GFO model, these two main bands are caused by absorption among the frontier molecular orbitals, from the HOMO and HOMO−1 orbitals to the LUMO and LUMO+1 orbitals. The two transitions in the *Q*-region are a result from a transition from two near-degenerate orbitals to the two LUMO orbitals. In the porphyrin system, for which the GFO model was originally developed, the latter band is significantly weaker in intensity that the Soret-band. This relative intensity is due to the near-degeneracy of the LUMO and LUMO+1 in the free base macrocycle, which leads to a cancellation of the transition moments in the *Q*-region, and a complementary strengthening of the transition moments in the Soret-region. However, it can be seen here that the intensities of the Soret- and *Q*-bands are relatively similar, in **Pc** as well as the **Pc** derivatives (Figures 4 and 5), which indicates a deviation from degeneracy of the LUMO orbitals, in the traditional, wave function-based, orbital picture. In DFT, however, the orbitals make little chemical sense, and in order to further analyze the nature of the transitions, the NTOs of a selection of compounds were calculated and plotted (Figure 4).

In the **Pc** core, it is seen that the transitions in the *Q*- and Soret-bands are mainly a result of electron density redistribution within the core aromatic structure, in accordance with the GFO model. However, a significant contribution can be seen from a transition from an orbital that mainly can be described as the HOMO+2 frontier orbital in one of the transitions in the Soret-band (<300 nm in Figure 4). This has led to suggestions that the GFO model might not be entirely suitable for the **Pc** core and its derivatives, and further investigations into the applicability of this model are being carried out in our group as well as others.[51]

It is worth noting at this stage that the NTOs give a suitable representation of the nature of the transitions to the *Q*- and Soret-bands. The OPA transitions in the substituted **Pc** derivatives were also analyzed using their NTOs, and examples of the plotted orbitals for an acceptor (**PcPN**) and donor complex (**PcCDMN**) are shown in Figure 5. It is clear that the absorption in the Soret- and *Q*-regions is mainly caused by transitions within the core aromatic structure, as in **Pc**. There is however evidence of charge transfer through the conjugated

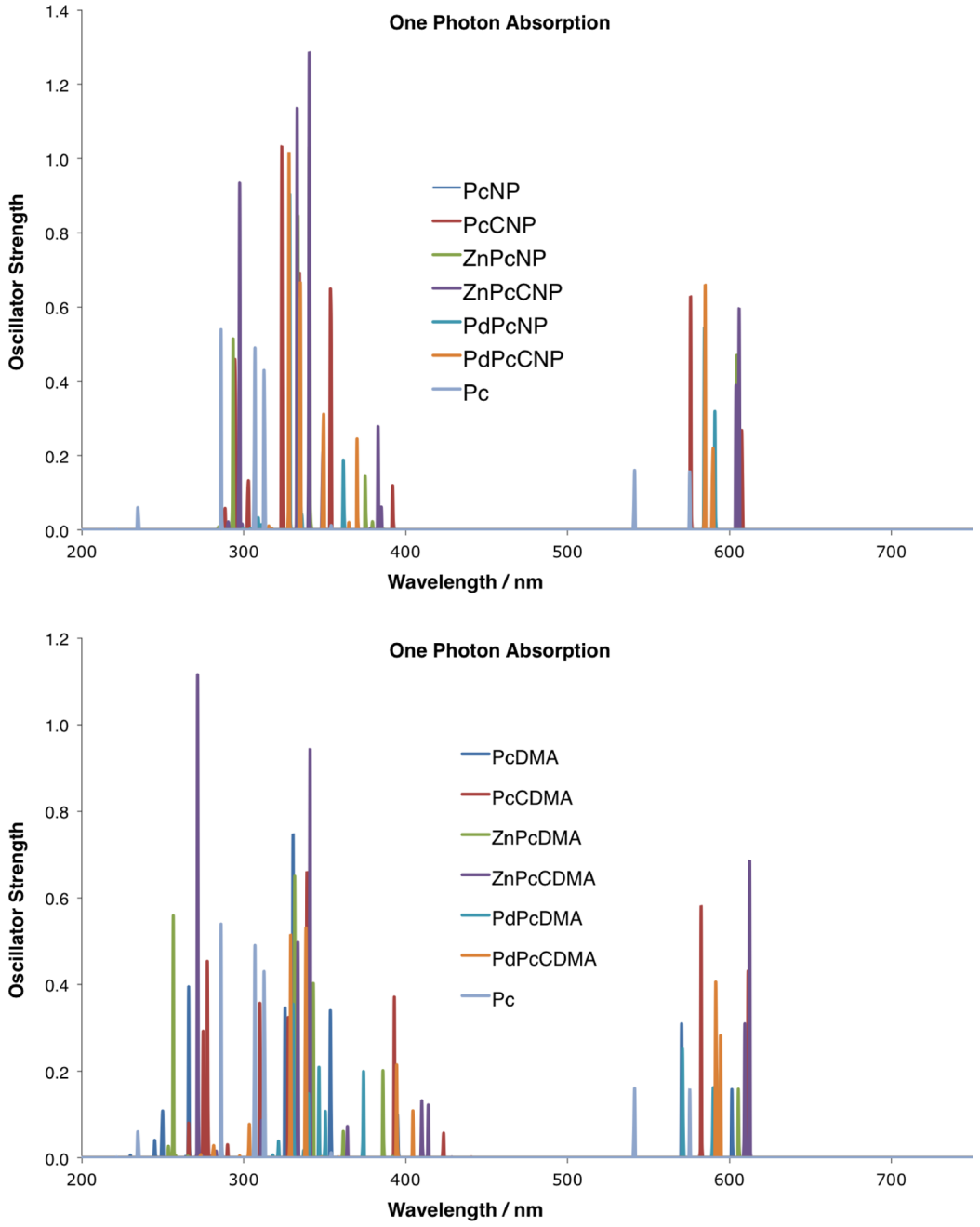

Figure 3. One-photon absorption results for **Pc**, as a free base or chelated to **Zn** or **Pd**, and its various nitrophenyl (**PN**) and dimethylamine (**DMA**) derivatives.

phenyl moiety to and from the electron accepting and donating substituents, respectively, at short wavelengths and also in the midwavelength region (at 280 and 380 nm, respectively, for both **PcNP** and **PcCDMN**).

For the species that contain a metal center, the same transition densities can be seen as for the transitions of the previously investigated structures in the *Q*-region and in the Soret. There is however significant contribution from absorption from two degenerate d-orbitals on the metal as well as from the substituents in the transitions in the Soret-region. This points to a further breakdown of the GFO model that becomes evident from the relative weakening in the intensity of the Soret-band for these derivatives.

Two-Photon Absorption. The TPA spectra from the quadratic response CAM-B3LYP/6-31G*,SDD calculations were simulated for 10 excited states of each irreducible representation of the point group that the optimized structures belong to. It is important to note that the wavelength of absorption presented is the total for the two-photon process, i.e., the results presented are the resonant absorption of two photons of equal wavelength.

The spectra all show a clear main absorption into the Soret-region, at 200−400 nm, and very small absorption into the *Q*-band. The effect of the substitution of the macrocycle is seen as a red-shift in the TPA maximum in all the structures investigated, compared to the free **Pc** macrocycle (Figures 6 and 7). Addition of an electron-withdrawing or -donating

dx.doi.org/10.1021/jp305063e | *J. Phys. Chem. B* 2012, 116, 11818−11828

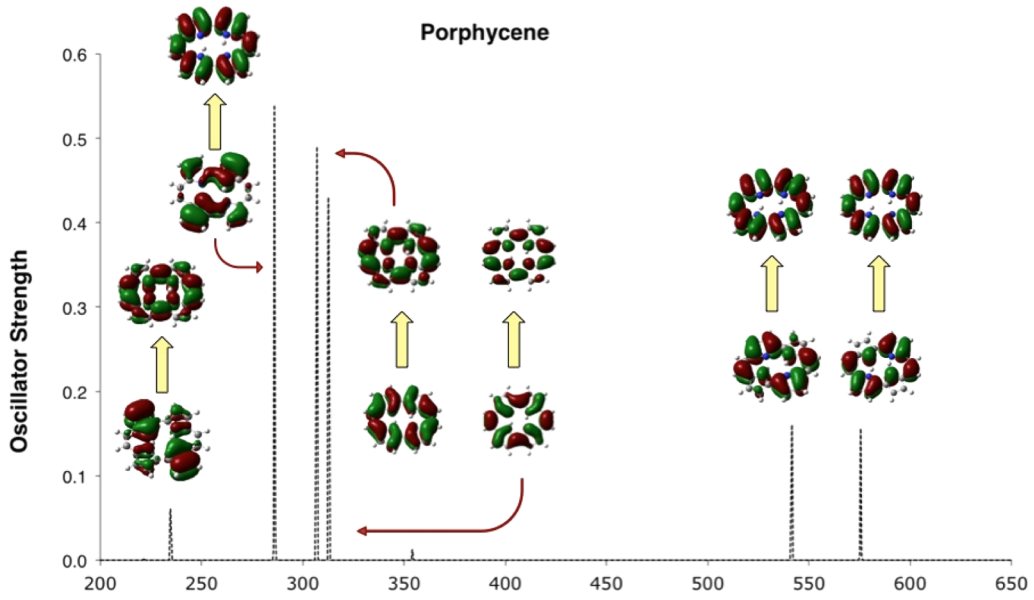

Figure 4. NTO representation of the transitions of free base **Pc**.

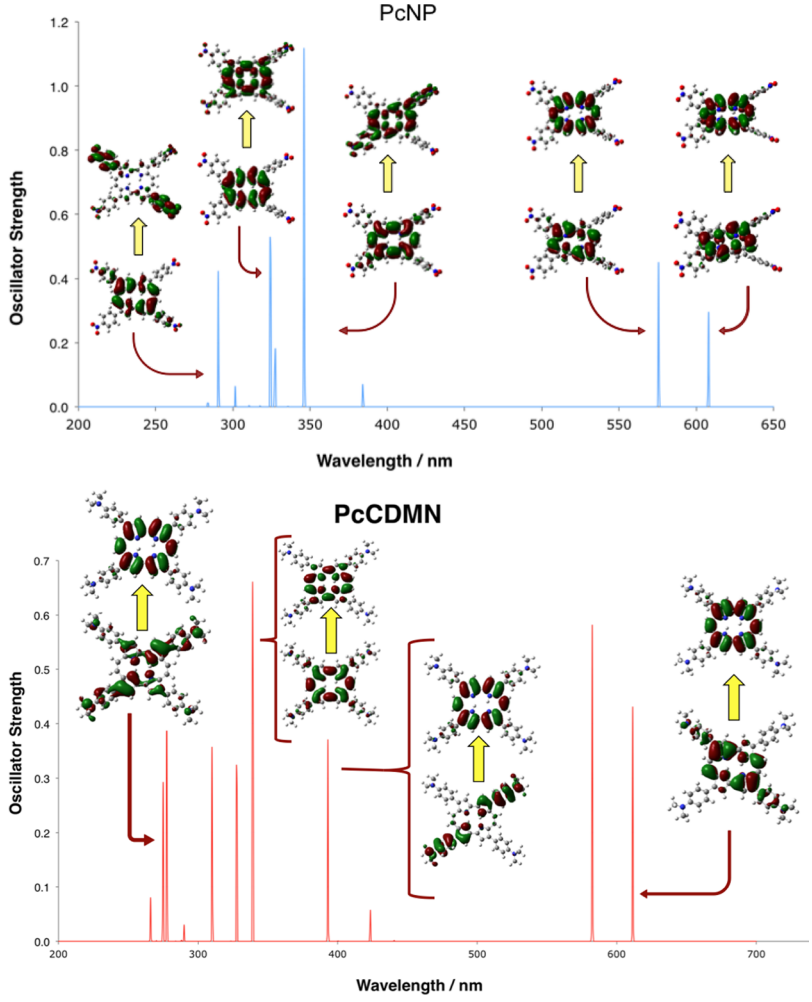

Figure 5. NTO representation of the transitions of **PcNP** and **PcCDMN**.

substituent leads to an absorption maximum in the region of 250−300 nm, which corresponds to a wavelength of incident light of 500−600 nm. This wavelength is approaching the optical window of tissue penetration, at 650−1300 nm, which is an encouraging result for applications in a biological environment. The chelation of the base to a Zn metal leads to an even

dx.doi.org/10.1021/jp305063e | J. Phys. Chem. B 2012, 116, 11818−11828

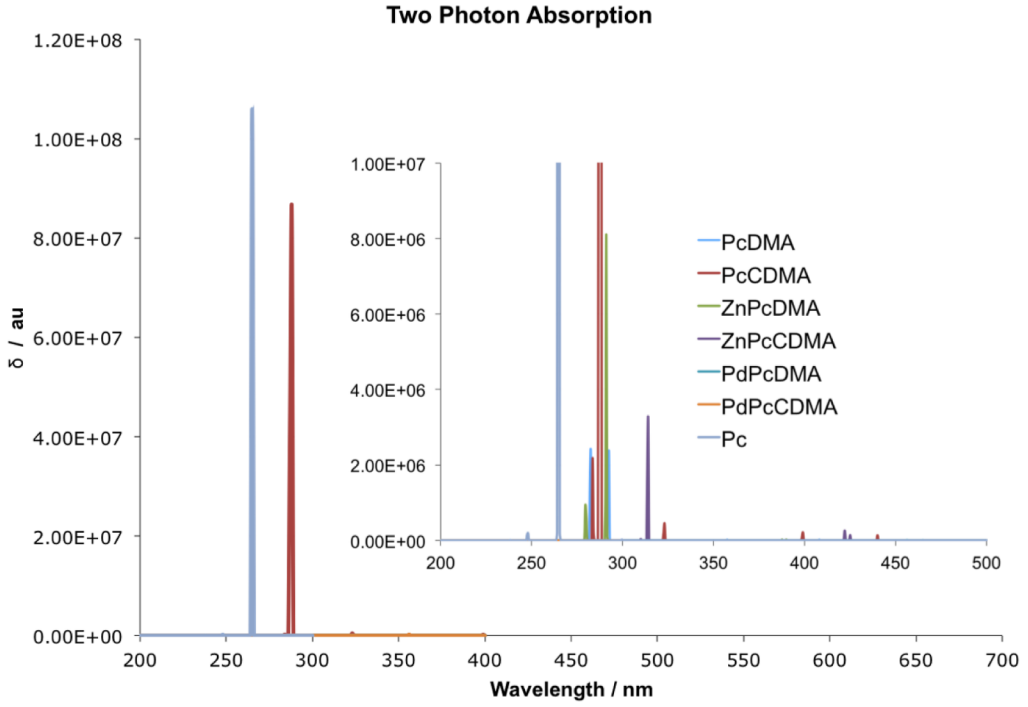

Figure 6. Two-photon absorption results for **Pc**, as a free base as well as chelated to **Zn** and **Pd** with **DMA** derivatives.

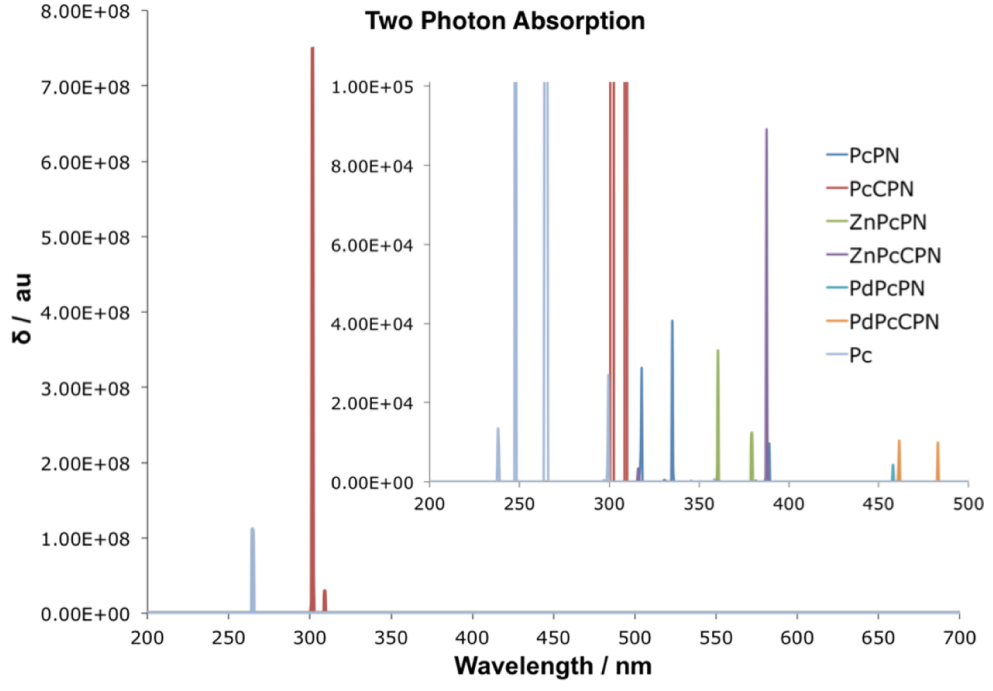

Figure 7. Two-photon absorption results for **Pc**, as a free base as well as chelated to **Zn** and **Pd** with **PN** derivatives.

larger red-shift with an absorption maximum at 370−390 nm. As the corresponding operating wavelength then would approach 740−780 nm, these molecules absorb well within the range of the optical window. With Pd coordinated to the center of the ring, the absorption maximum is further red-shifted, 350−450 nm, corresponding to an operating wavelength of up to 900 nm. This wavelength is in an even more preferable position in the tissue penetration window, as the absorption due to various chromophores is approaching an absolute minimum at this point. For the application of the compounds as photosensitizers for future use in PDT, the wavelength of maximum absorption is indeed crucial, but an optimal photosensitizer must also have a high TPA cross section in the relevant region.

The TPA cross section, δ, in the investigated compounds is improved by addition of electron-withdrawing groups compared to the free **Pc** molecule. However, the increase is only evident when substituents are separated from the macrocyclic structure by a π-bridge that extends the conjugation of the system. The reason for the effect of the addition of substituents

dx.doi.org/10.1021/jp305063e | J. Phys. Chem. B 2012, 116, 11818−11828

in this manner is the increased transition dipole moment. As this will lead to an increase in the transition matrix element, T, it becomes evident from eq 1 that an increase in the TPA cross section will occur as a result. The very large cross section of the TPA of the **Pc** free base macrocycle, as well as for **PcCPN** and **PcCDMA**, when comparing to the alternative molecular structures can be explained in terms of one-photon resonance enhancement of the transition. The phenomenon of resonance enhancement is best illustrated by consideration of the sum-over-states expression seen in eq 2 .The magnitude of T depends on the difference of the v-th state and the frequency of the total excitation through the denominator in the expression, $(\omega_v - \omega)$, which will approach zero if the frequency of the incident light approaches the frequency difference between the intermediate and the ground state. Since the intermediate state is a linear combination of all real eigenstates of the system, a TPA transition that proceeds through an intermediate state that can be described mainly in terms of a real state will be significantly enhanced. An allowed OPA Q-transition accidentally degenerate at half the Soret-transition energy will therefore greatly enhance the TPA transition into the Soret-band. The effect of resonance enhancement is clearly seen in the case of the free **Pc** macrocycle as well as **PcCPN** and **PcCDMA** but also, to a lesser extent, in the Zn-chelated compounds, as displayed in Table 2. The values of the δ at wavelengths that are near or at resonance cannot be determined explicitly, as evident from eq 2, using the method described here but are useful in the interpreting of general trends in the TPA spectra. The wavelengths of maximum TPA in the Soret-region for these systems are very nearly in resonance with an allowed OPA in the Q-region, which leads to the conclusion that the δ in the Soret-region should be very large. This is not the case for any of the other systems, which rationalizes the comparably low TPA cross sections for these species. Resonance enhancement also rationalizes why there are only very weak TPA transitions to be seen in the Q-region for any of the investigated photosensitizers, as there is no allowed one-photon transition near half the wavelength value of this region. The effect of large structural changes like these on the TPA cross section, especially as a cause of resonance enhancement, is also supported by experimental studies. This highlights the fact that a theoretical input could be crucial in studies such as these, where the photosensitizers are challenging synthetic targets, as well as studies where new structure−TPA relationships are being investigated. An example of the latter is the investigation into the effect of the substitution of core heteroatoms in a macrocycle on the TPA cross section, carried out by us, where the TPA was shown to be surprisingly sensitive to such structural changes.[20]

Table 2. Wavelengths (nm) of Maximum TPA and OPA for the Various Species in the Soret- and Q-Region[a]

	OPA maxima		TPA maxima
	Soret	Q	Soret
Pc	320	**530**	**265**
PcPN	345	575	300
PcCPN	360	**580**	**300**
ZnPcPN	340	595	365
ZnPcCPN	360	600	390
PdPcPN	355	585	465
PdPcCPN	370	585	470
PcDMA	330	570	282
PcCDMA	339	**582**	**287**
ZnPcDMA	331	592	290
ZnPcCDMA	340	**612**	**313**
PdPcDMA	330	571	456
PdPcCDMA	338	591	482

[a]Marked in bold are the transition wavelengths that are in near-resonance.

Solvation Effects. The effect of a solvent on the OPA spectra was calculated using the PCM to simulate water surroundings, on PCM optimized geometries using the Gaussian 09 standard static and optical dielectric constants of 78.36 and 1.78, respectively. In the resulting absorption spectra, for the OPA transitions, two general trends can be seen in terms of the oscillator strength of the transition. For the compounds with a phenyl moiety, extending the conjugation of the chromophore, the main transition into the Soret-band is significantly enhanced, as demonstrated in Figure 8. This is also the case in compounds chelated to a Pd metal center. Enhanced absorption points to the fact that the solvent has a positive effect on the difference in dipole moment between the ground and the Soret-state in going from the gas to the solution phase, and has been demonstrated for porphyrins in previous PCM studies.[52]

The analysis of the solvatochromic shifts shows only a very slight change in all the bands for all chromophores, which does not impact the OPA transitions to a very large degree. However, it is important to keep in mind that these small solvatochromic shifts in the states are also valid for the TPA transitions. This is pertinent in that it has been shown that only a small shift in the position of the Q-band can have a very large impact on the TPA into the Soret-band, through a resonance enhanced transition.

CONCLUSION

This work utilized linear and quadratic density functional response theory to display the effects of structure on OPA and TPA characteristics in substituted **Pc** photosensitizers. From the linear response results, the expected spectral pattern could be seen in two clear Soret- and Q-bands in the absorption spectra for all the investigated **Pc** derivatives. These bands are well characterized for the free base porphyrin, using the classic Gouterman model. Analysis of the NTOs of these bands for the **Pc** systems investigated here, however, suggests that this classic model might not give a complete picture of the transitions in **Pc**. Specifically, the model does not account for the relative intensities of the Soret- and Q-bands, that differ from the parent porphyrin system. Both the OPA and TPA results demonstrate that the **Pc** macrocycle has a range of promising attributes for use as an agent in photodynamic therapy as both one- and two-photon activated photosensitizer. In particular, the use of TPA to tune the maximum wavelength of absorption to within the optical window of tissue penetration is predicted to be very fruitful for this series of **Pc** derivatives. This was achieved through the coordination of **Pc** at a Zn or Pd metal center. A very large increase in TPA cross section was displayed for derivatives bearing electron withdrawing or donating substituents where the chromophore was extended in order to facilitate large charge transfer during the transition. The phenomenon of resonance enhancement plays a significant role in contributing to the very large TPA cross section values that could be seen. Future research into TPA PDT should aim at the development of structures that exhibit strong resonance

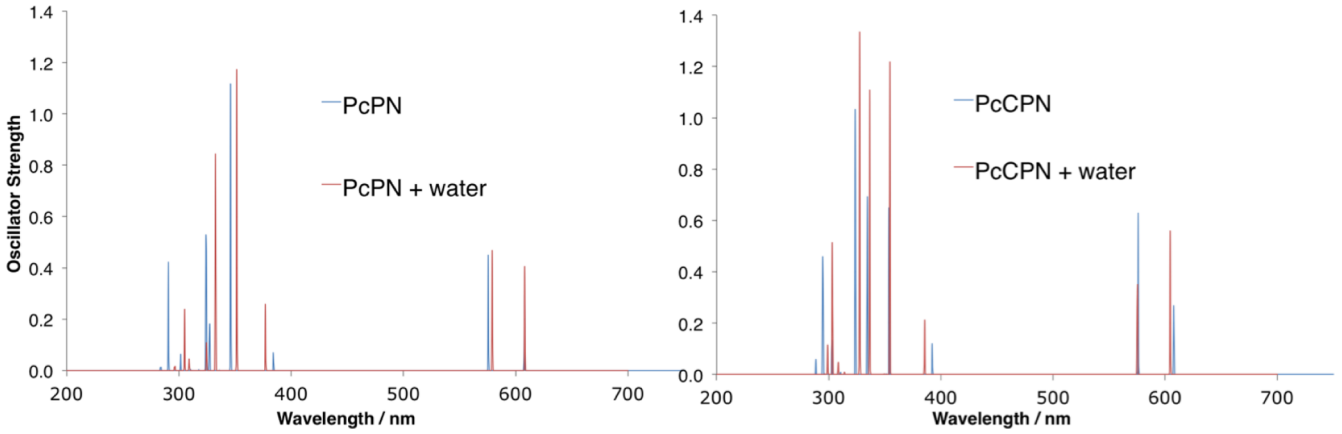

Figure 8. OPA results with and without water surroundings for **PcPN** and **PcCPN**.

enhancement as well as an absorption maximum within the optical window of tissue penetration. The solvent effects demonstrated using the PCM on the OPA transitions are small but need to be taken into account, as very small effects on the OPA spectra can still afford very large changes in the TPA spectra. Future research should also aim at incorporating TPA solvent studies, as well as the use of more specific models, such as QM/MM in order to fully appreciate the extent of these effects. The theoretical data presented here indicates that there is a large amount of information to be gained on the photochemical behavior of relatively large chromophores from computations. These results can then be used as foundations for future experimental research, and a theoretical input has the potential to greatly drive the development of photosensitizer agents.

AUTHOR INFORMATION

Corresponding Author

*E-mail: m.j.paterson@hw.ac.uk.

Notes

The authors declare no competing financial interest.

ACKNOWLEDGMENTS

This work was supported by the European Research Council under the European Union's Seventh Framework Programme (FP7/2007-2013/ERC Grant agreement number: 258990).

REFERENCES

(1) He, G. S.; Tan, L.-S.; Zheng, Q.; Prasad, P. N. *Chem. Rev.* **2008**, *108*, 1245−1330.
(2) Parthenopoulos, D. A.; Rentzepis, P. M. *Science* **1989**, *245*, 843−845.
(3) Dvornikov, A. S.; Walker, E. P.; Rentzepis, P. M. *J. Phys. Chem. A* **2009**, *113*, 13633−13644.
(4) Larson, D. R.; Zipfel, W. R.; Williams, R. M.; Clark, S. W.; Bruchez, M. P.; Wise, F. W.; Webb, W. W. *Science* **2003**, *300*, 1434−1436.
(5) Bhawalkar, J. D.; Kumar, N. D.; Zhao, C. F.; Prasad, P. N. *J. Clin. Laser Med. Surg.* **1997**, *15*, 201−204.
(6) Ogawa, K.; Kobuke, Y. *Anticancer Agents Med. Chem.* **2008**, *8*, 269−279.
(7) Schuitmaker, J. J.; Baas, P.; van Leengoed, H. L.; van der Meulen, F. W.; Star, W. M.; van Zandwijk, N. *J. Photochem. Photobiol., B* **1996**, *34*, 3−12.
(8) Bonnett, R. *Chemical Aspects of Photodynamic Therapy*; Gordon and Breach Science Publishers: Amsterdam, The Netherlands, 2000.
(9) Almeida, R. D.; Manadas, B. J.; Carvalho, A. P.; Duarte, C. B. *Biochim. Biophys. Acta* **2004**, *1704*, 59−86.
(10) Oleinick, N. L.; Morris, R. L.; Belichenko, I. *Photochem. Photobiol. Sci.* **2002**, *1*, 1−21.
(11) Frederiksen, P. K.; Jorgensen, M.; Ogilby, P. R. *J. Am. Chem. Soc.* **2001**, *123*, 1215−1221.
(12) Bhawalkar, J. D.; Kumar, N. D.; Zhao, C. F.; Prasad, P. N. *J. Clin. Laser Med. Surg.* **1997**, *15*, 201−204.
(13) Karotki, A.; Khurana, M.; Lepock, J. R.; Wilson, B. C. *Photochem. Photobiol.* **2006**, *82*, 443−452.
(14) Fisher, W. G.; Partridge, W., Jr.; Dees, C.; Wachter, E. A. *Photochem. Photobiol.* **1997**, *66*, 141−155.
(15) Arnbjerg, J.; Jimenez-Banzo, A.; Paterson, M. J.; Nonell, S.; Borrell, J. I.; Christiansen, O.; Ogilby, P. R. *J. Am. Chem. Soc.* **2007**, *129*, 5188−5199.
(16) Dolphin, D.; Sternberg, E. D.; Bruckner, C. *Tetrahedron* **1998**, *54*, 4151−4202.
(17) Sanchez-Garcia, D.; Sessler, J. L. *Chem. Soc. Rev.* **2008**, *37*, 215−232.
(18) Kim, K. S.; Sung, Y. M.; Matsuo, T.; Hayashi, T.; Kim, D. *Chemistry* **2011**, *17*, 7882−7889.
(19) Stockert, J. C.; Canete, M.; Juarranz, A.; Villanueva, A.; Horobin, R. W.; Borrell, J. I.; Teixido, J.; Nonell, S. *Curr. Med. Chem.* **2007**, *14*, 997−1026.
(20) Bergendahl, L. T.; Paterson, M. J. *Chem. Commun.* **2012**, *48*, 1544−1546.
(21) Norman, P. *Phys. Chem. Chem. Phys.* **2011**, *13*, 20519−20535.
(22) Bast, R.; Ekstrom, U.; Gao, B.; Helgaker, T.; Ruud, K.; Thorvaldsen, A. J. *Phys. Chem. Chem. Phys.* **2011**, *13*, 2627−2651.
(23) Poulsen, T. D.; Frederiksen, P. K.; Jorgensen, M.; Mikkelsen, K. V.; Ogilby, P. R. *J. Phys. Chem. A* **2001**, *105*, 11488−11495.
(24) Salek, P.; Vahtras, O.; Guo, J.; Luo, Y.; Helgaker, T.; Agren, H. *Chem. Phys. Lett.* **2003**, *374*, 446−452.
(25) Zhou, X.; Feng, J.-K.; Ren, A.-M. *Chem. Phys. Lett.* **2004**, *397*, 500−509.
(26) Dahlstedt, E.; Collins, H. A.; Balaz, M.; Kuimova, M. K.; Khurana, M.; Wilson, B. C.; Phillips, D.; Anderson, H. L. *Org. Biomol. Chem.* **2009**, *7*, 897−904.
(27) Albota, M.; et al. *Science* **1998**, *281*, 1653−1656.
(28) Shen, J.; Cheng, W.-D.; Wu, D.-S.; Lan, Y.-Z.; Li, F.-F.; Huang, S.-P.; Zhang, H.; Gong, Y.-J. *J. Phys. Chem. A* **2006**, *110*, 10330−10335.
(29) Drobizhev, M.; Meng, F. Q.; Rebane, A.; Stepanenko, Y.; Nickel, E.; Spangler, C. W. *J. Phys. Chem. B* **2006**, *110*, 9802−9814.
(30) Drobizhev, M.; Stepanenko, Y.; Dzenis, Y.; Karotki, A.; Rebane, A.; Taylor, P. N.; Anderson, H. L. *J. Phys. Chem. B* **2005**, *109*, 7223−7236.
(31) Pawlicki, M.; Collins, H. A.; Denning, R. G.; Anderson, H. L. *Angew. Chem., Int. Ed. Engl.* **2009**, *48*, 3244−3266.

(32) Ogawa, K.; Hasegawa, H.; Inaba, Y.; Kobuke, Y.; Inouye, H.; Kanemitsu, Y.; Kohno, E.; Hirano, T.; Ogura, S.-I.; Okura, I. *J. Med. Chem.* **2006**, *49*, 2276−2283.
(33) Ray, P. C.; Sainudeen, Z. *J. Phys. Chem. A* **2006**, *110*, 12342−12347.
(34) Rubio-Pons, O.; Luo, Y.; Agren, H. *J. Chem. Phys.* **2006**, *124*, 94310.
(35) Improta, R.; Ferrante, C.; Bozio, R.; Barone, V. *Phys. Chem. Chem. Phys.* **2009**, *11*, 4664−4673.
(36) Tomasi, J.; Mennucci, B.; Cammi, R. *Chem. Rev.* **2005**, *105*, 2999−3093.
(37) Hehre, W. J.; Ditchfield, R.; Pople, J. A. *J. Chem. Phys.* **1972**, *56*, 2257−2261.
(38) Hariharan, P. C.; Pople, J. A. *Theor. Chim. Acta* **1973**, *28*, 213−222.
(39) Andrae, D.; Haussermann, U.; Dolg, M.; Stoll, H.; Preuss, H. *Theor. Chim. Acta* **1990**, *77*, 123−141.
(40) Frisch, M. J.; et al. *Gaussian 09*, revision A.2; Gaussian, Inc.: Wallingford, CT, 2009.
(41) DALTON, a molecular electronic structure program, Release 2.0 (2005), see http://daltonprogram.org/.
(42) Becke, A. D. *J. Chem. Phys.* **1993**, *98*, 5648−5652.
(43) Yanai, T.; Tew, D.; Handy, N. *Chem. Phys. Lett.* **2004**, *939*, 51−57.
(44) Peach, M. J. G.; Helgaker, T.; Salek, P.; Keal, T. W.; Lutnaes, O. B.; Tozer, D. J.; Handy, N. C. *Phys. Chem. Chem. Phys.* **2006**, *8*, 558−562.
(45) Paterson, M. J.; Christiansen, O.; Pawlowski, F.; Jorgensen, P.; Hattig, C.; Helgaker, T.; Salek, P. *J. Chem. Phys.* **2006**, *124*, 054322.
(46) Martin, R. L. *J. Chem. Phys.* **2003**, *118*, 4775−4777.
(47) Paterson, M. J.; Kongsted, J.; Christiansen, O.; Mikkelsen, K. V.; Nielsen, C. B. *J. Chem. Phys.* **2006**, *125*, 184501.
(48) Ferrighi, L.; Frediani, L.; Fossgaard, E.; Ruud, K. *J. Chem. Phys.* **2007**, *127*, 244103.
(49) Luo, Y.; Norman, P.; Macak, P.; Agren, H. *J. Phys. Chem. A* **2000**, *104*, 4718−4722.
(50) Milgrom, L. R. *The Colours of Life - An introduction to the chemistry of porphyrins and Related Compounds*; Oxford University Press: Oxford, 1997.
(51) Hasegawa, J.-y.; Takata, K.; Miyahara, T.; Neya, S.; Frisch, M. J.; Nakatsuji, H. *J. Phys. Chem. A* **2005**, *109*, 3187−3200.
(52) Venkataramanan, N. S.; Suvitha, A.; Nejo, H.; Mizuseki, H.; Kawazoe, Y. *Int. J. Quantum Chem.* **2011**, *111*, 2340−2351.